Volume 13
Number 42
14 November 2022
Pages 12247–12590

Chemical Science

rsc.li/chemical-science

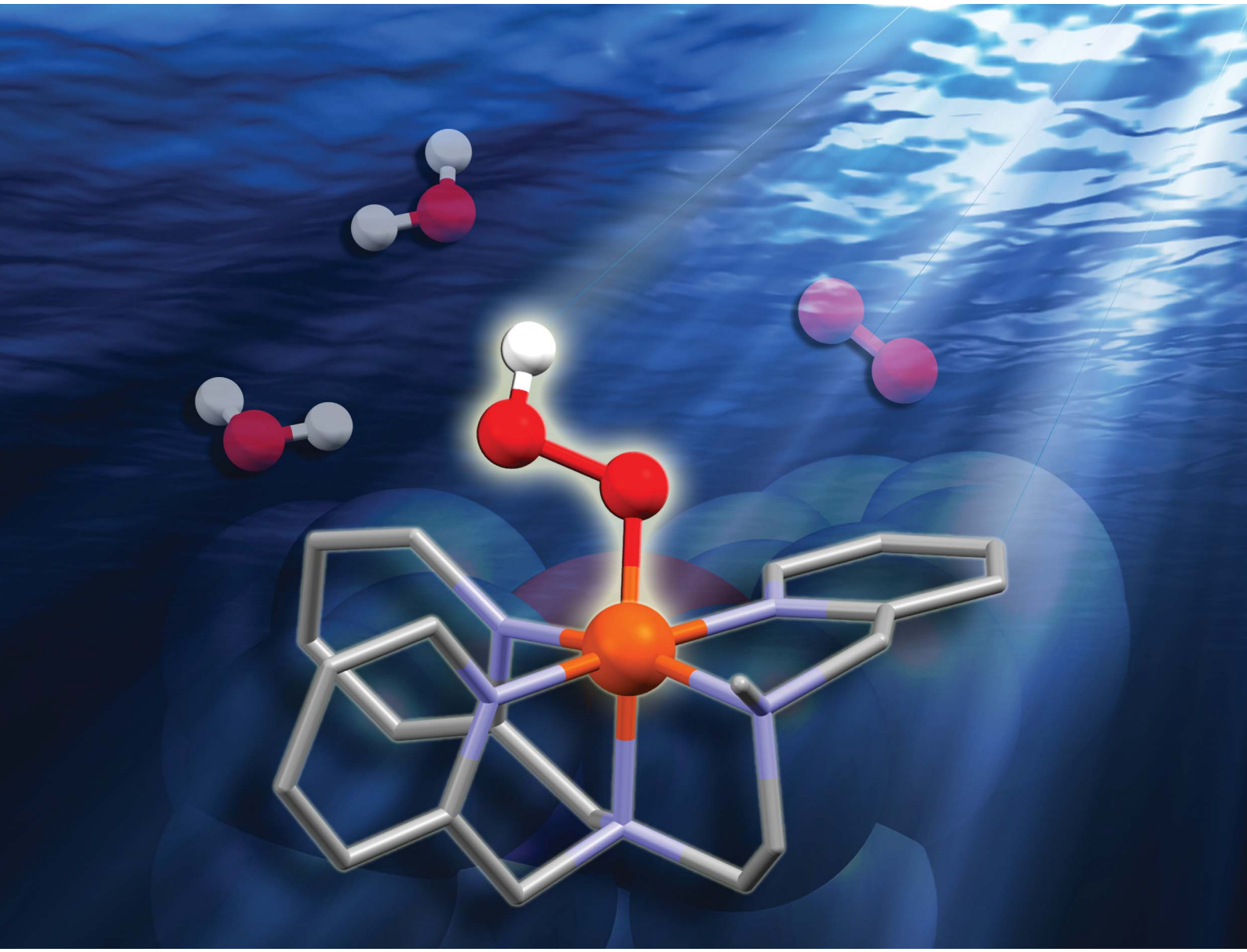

ISSN 2041-6539

ROYAL SOCIETY OF CHEMISTRY

EDGE ARTICLE

Winfried Leibl, Ally Aukauloo *et al.*
Photocatalytic generation of a non-heme Fe(III)-hydroperoxo species with O_2 in water for the oxygen atom transfer reaction

Chemical Science

ROYAL SOCIETY OF CHEMISTRY

EDGE ARTICLE

View Article Online
View Journal | View Issue

Cite this: *Chem. Sci.*, 2022, **13**, 12332

All publication charges for this article have been paid for by the Royal Society of Chemistry

Photocatalytic generation of a non-heme Fe(III)-hydroperoxo species with O_2 in water for the oxygen atom transfer reaction†

Eva Pugliese, [a] Nhat Tam Vo,[a] Alain Boussac, [b] Frédéric Banse, [a] Yasmina Mekmouche, [c] Jalila Simaan, [c] Thierry Tron, [c] Philipp Gotico, [b] Marie Sircoglou, [a] Zakaria Halime, [a] Winfried Leibl *[b] and Ally Aukauloo *[ab]

Coupling a photoredox module and a bio-inspired non-heme model to activate O_2 for the oxygen atom transfer (OAT) reaction requires a vigorous investigation to shed light on the multiple competing electron transfer steps, charge accumulation and annihilation processes, and the activation of O_2 at the catalytic unit. We found that the efficient oxidative quenching mechanism between a $[Ru(bpy)_3]^{2+}$ chromophore and a reversible electron mediator, methyl viologen (MV^{2+}), to form the reducing species methyl viologen radical ($MV^{\bullet+}$) can convey an electron to O_2 to form the superoxide radical and reset an Fe(III) species in a catalytic cycle to the Fe(II) state in an aqueous solution. The formation of the Fe(III)-hydroperoxo (Fe^{III}–OOH) intermediate can evolve to a highly oxidized iron-oxo species to perform the OAT reaction to an alkene substrate. Such a strategy allows us to bypass the challenging task of charge accumulation at the molecular catalytic unit for the two-electron activation of O_2. The Fe^{III}–OOH catalytic precursor was trapped and characterized by EPR spectroscopy pertaining to a metal assisted catalysis. Importantly, we found that the substrate itself can act as an electron donor to reset the photooxidized chromophore in the initial state closing the photocatalytic loop and hence excluding the use of a sacrificial electron donor. Laser Flash Photolysis (LFP) studies and spectroscopic monitoring during photocatalysis lend credence to the proposed catalytic cycle.

Received 1st June 2022
Accepted 27th September 2022

DOI: 10.1039/d2sc03129a

rsc.li/chemical-science

Introduction

The dioxygen molecule is undoubtedly the most environmentally compatible oxidant. Due to its triplet ground state, it does not readily oxidize diamagnetic organic compounds. Nature has developed both heme[1–3] and non-heme enzymes[4–6] to activate O_2 through electron and proton transfers for essential oxidative metabolism and chemical transformations such as oxygen atom transfer (OAT) reactions as summarized in the following equation (S = substrate and SO = oxygenated substrate):

$$S + O_2 + 2e^- + 2H^+ \rightarrow SO + H_2O$$

Chemists have taken inspiration from biology to develop metal complexes that can bind and activate dioxygen in the presence of co-reductants or with added hazardous oxidants to form active metal–oxygen intermediates such as metal-peroxo or metal-oxo species capable of realizing OAT reactions.[5,7–20] The electrochemical activation of O_2 in the presence of a metal catalyst has also been pursued and is currently regaining much momentum. This approach relies on the electro-generation of superoxide or H_2O_2 at the surface of an electrode that ultimately reacts with the metal catalyst to form highly active metal-(hydro) peroxo species. This route too faces different challenges such as reducing the active metal-(hydro)peroxo intermediates or intermolecular reactions leading to unreactive bridged oxo metal complexes.[6,21–30]

An alternative route to develop more sustainable processes relies on the coupling of a photoredox module and a molecular transition metal catalyst for photocatalytic OAT reactions.[31–43] The activation of O_2 through light-induced electron transfer provides a unique opportunity to generate these reactive oxo and peroxo species in a benign and controlled manner.[44–48] This quest comes along with more challenges on top of those of the classic chemical approaches. Indeed, light-induced electron transfer from the excited state of the photosensitizer module must be steered in a directional way towards the molecular

[a]*Institut de Chimie Moléculaire et des Matériaux d'Orsay, UMR 8182, Université Paris-Saclay, CNRS, F-91405 Orsay Cedex, France. E-mail: ally.aukauloo@universite-paris-saclay.fr*

[b]*Université Paris-Saclay, CEA, CNRS, Institute for Integrative Biology of the Cell (I2BC), F-91191 Gif-sur-Yvette, France. E-mail: winfried.leibl@cea.fr*

[c]*Aix Marseille Université, Centrale Marseille, CNRS, ISM2 UMR 7313, 13397, Marseille, France*

† Electronic supplementary information (ESI) available. See https://doi.org/10.1039/d2sc03129a

catalyst for charge accumulation and O_2 activation to further carry out multi-electron catalysis. Recent efforts in this exploration have paved the way for using light and O_2 to oxygenate different substrates in a selective manner.[46,49]

König and coworkers reported the photocatalytic oxidation of ethyl benzenes to the corresponding ketone and benzyl alcohols to benzaldehydes with riboflavin tetraacetate (RFT), where O_2 acts as the sacrificial electron acceptor to form H_2O_2 and regenerate RFT.[50] The H_2O_2 formed was found to ultimately degrade RFT. In a subsequent study, Wolf and colleagues astutely took profit of this deleterious by-product in a dual catalytic system containing both the RFT and a non-heme iron(II) complex, $[(TPA)Fe^{II}]^{2+}$ (TPA = tris(2-pyridylmethyl)amine). The latter acted as a fuse to protect the photoredox RFT by reacting with the *in situ* generated H_2O_2 to form the active iron(III)-hydroperoxo species, $[(TPA)Fe^{III}(OOH)]^{2+}$, that participates in the photocatalytic cycle for the oxygenation of alkyl benzene.[51] However, insights into the photoredox activation of O_2 at a metal complex are yet to be deciphered.

In this study, we used the well-known ruthenium(II) trisbipyridine, ($[Ru^{II}(bpy)_3]^{2+}$), as a photosensitizer because of its unique photophysical properties (a long life time of the excited state), its solubility in an aqueous medium, and the redox activity of the exited state together with the high oxidative potential of the oxidized form of the chromophore.[52,53] Reversible electron acceptors such as methyl viologen (MV^{2+}) are commonly used in light-induced electron transfer processes producing the oxidized photosensitizer, *i.e.*, $[Ru^{III}(bpy)_3]^{3+}$ from $[Ru^{II}(bpy)_3]^{2+}$ and the reduced methyl viologen radical ($MV^{\bullet+}$) through an oxidative quenching mechanism.[54,55] These photoreactions are normally carried out in the absence of O_2 as the latter can interfere with the excited triplet state of the chromophore and importantly, can snatch an electron from $MV^{\bullet+}$ to form $O_2^{\bullet-}$ leading to subsequent reactions.[56] We have been interested in taking profit of the reducing power of photogenerated $MV^{\bullet+}$ ($E^\circ = -653$ mV *vs.* Ag/AgCl)[57] to activate concomitantly an O_2 molecule to form the superoxide anion ($O_2^{\bullet-}$) and resetting a non-heme Fe(III) intermediate at the closure of an OAT catalytic cycle to the corresponding Fe(II) form. The chemical reaction between the photogenerated Fe(II) form and $O_2^{\bullet-}$ should under the right pH conditions reinject the active iron(III)-hydroperoxo intermediate, Fe^{III}–OOH, into the catalytic loop. Such an approach should allow us to bypass the challenging task of charge accumulation at the molecular catalytic unit for the two-electron activation of O_2 for OAT reactions.

We report here the photocatalytic activity in an aqueous solution of a mixture of $[Ru^{II}(bpy)_3]^{2+}$/$[(L_5)Fe^{II}]^{2+}$/MV^{2+} in the presence of O_2 as an oxygen atom source towards the OAT reaction to an alkene as a substrate as sketched in Scheme 1. To accomplish this task, we used an air-stable non-heme $[(L_5)Fe^{II}]^{2+}$ model catalyst (where L_5 stands for *N*,*N*′,*N*′-tris(2-pyridylmethyl)ethane-1,2-diamine) (see Scheme 1). The choice of this complex was guided by the numerous studies done on the activation of O_2 and H_2O_2.[58–60] Photocatalytic runs demonstrated the oxygenation of styrene sulfonate in water to yield the corresponding epoxide or diol and the use of $^{18}O_2$ indicated that O_2 is the source of the inserted oxygen atom. Importantly, we have captured the Electron Paramagnetic Resonance (EPR) signals of both the high-spin $[(L_5)Fe^{III}$–$\eta^2O_2]^+$ and the low-spin $[(L_5)Fe^{III}$–$OOH]^{2+}$ species as observed for the chemically generated catalytically active forms under the right pH control.[58,59] In what follows, we discuss the photoredox events that allow us to provide insights into the photocatalytic OAT reaction.

Results and discussion

Laser Flash Photolysis (LFP) experiments helped us to decipher the photochemical events and confirm the implication of both the methyl viologen and the iron catalyst in the activation process of O_2 for the OAT reaction. Under our experimental conditions at pH 4, the catalyst is initially mainly present in its $[(L_5)Fe^{II}$–$OH_2]^{2+}$ form (herein denoted as $[(L_5)Fe^{II}]^{2+}$).

(i) Under anaerobic conditions and in the absence of the iron complex, the emission of the $[Ru^{II}(bpy)_3]^{2+}$* excited state was notably quenched by the addition of MV^{2+} (eqn (2)) with a shortening of the lifetime of the excited state from 600 ns to 270 ns.

$$[Ru^{II}(bpy)_3]^{2+} + h\nu \rightarrow [Ru^{II}(bpy)_3]^{2+*} \quad (1)$$

$$[Ru^{II}(bpy)_3]^{2+*} + MV^{2+} \rightarrow [Ru^{III}(bpy)_3]^{3+} + MV^{\bullet+} \quad (2)$$

This event can be monitored by the appearance of the characteristic absorption bands of $MV^{\bullet+}$ (390 and 605 nm) and the disappearance of the MLCT band of $[Ru^{II}(bpy)_3]^{2+}$ at 450 nm attesting the formation of the highly oxidizing $[Ru^{III}(bpy)_3]^{3+}$ (Fig. S1†). Both species disappeared by charge recombination (eqn (2′)) on the ms time scale (Fig. S2,† blue and red traces).

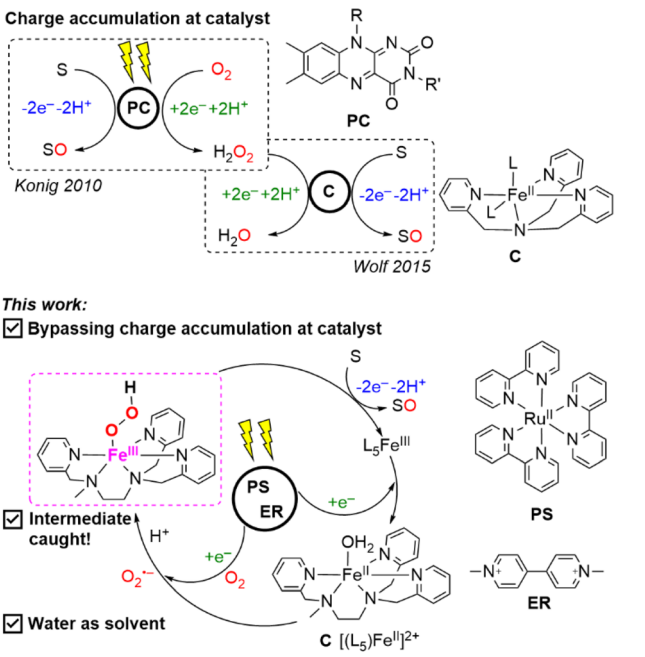

Scheme 1 (Top) reported strategy of accumulating charges on a photocatalyst (PC) or catalyst (C) to perform oxygen atom transfer (S = substrate and SO = oxygenated substrate) in comparison to (bottom) the strategy employed in this paper of bypassing charge accumulation using stepwise charge transfers in the photosensitizer (PS), electron relay (ER), substrate, and catalyst.

$$[Ru^{III}(bpy)_3]^{3+} + MV^{\bullet+} \rightarrow [Ru^{II}(bpy)_3]^{2+} + MV^{2+} \quad (2')$$

(ii) In the presence of O_2, we observed an accelerated decay of $MV^{\bullet+}$ compared to anaerobic conditions. This demonstrates rapid electron transfer from $MV^{\bullet+}$ to O_2 forming $O_2^{\bullet-}$ (eqn (3), Fig. S2,† orange trace).

$$MV^{\bullet+} + O_2 \rightarrow MV^{2+} + O_2^{\bullet-} \quad (3)$$

The formation of superoxide radicals *via* $MV^{\bullet+}$ in aqueous solution has been described in a recent study under similar conditions.[61] It should be noted that the fast quenching of the $[Ru^{II}(bpy)_3]^{2+}$* excited triplet state by MV^{2+} (present at a concentration nearly two orders of magnitude higher than the concentration of O_2) minimizes the formation of singlet oxygen *via* triplet–triplet energy transfer from $[Ru^{II}(bpy)_3]^{2+}$* to $^3O_2$. Back electron transfer from $O_2^{\bullet-}$ to $[Ru^{III}(bpy)_3]^{3+}$ (eqn (4)) occurs with similar kinetics to those between $MV^{\bullet+}$ and $[Ru^{III}(bpy)_3]^{3+}$ in the absence of O_2 (Fig. S2,† cyan trace).

$$[Ru^{III}(bpy)_3]^{3+} + O_2^{\bullet-} \rightarrow [Ru^{II}(bpy)_3]^{2+} + O_2 \quad (4)$$

(iii) Excitation of $[Ru^{II}(bpy)_3]^{2+}/MV^{2+}$ in the absence of O_2 but in the presence of 4-styrenesulfonate as the substrate (herein denoted as S) leads to the faster recovery of $[Ru^{II}(bpy)_3]^{2+}$ than with $MV^{\bullet+}$ only (Fig. S3†). This observation can be explained by the intermolecular oxidation of S by $[Ru^{III}(bpy)_3]^{3+}$ to generate an alkenyl radical (eqn (5)) as certified when S was treated by chemically prepared $[Ru^{III}(bpy)_3]^{3+}$ (Fig. S14†).

$$[Ru^{III}(bpy)_3]^{3+} + S \rightarrow [Ru^{II}(bpy)_3]^{2+} + S^{\bullet+} \quad (5)$$

(iv) No modification of the $[Ru^{II}(bpy)_3]^{2+}$* excited state lifetime was noticed in the presence of the iron complex only (Fig. S4†). This indicates that there is no direct activation of the iron complex from the excited triplet state of the photosensitizer neither through electron nor energy transfer processes. The excitation of a mixture of $[Ru^{II}(bpy)_3]^{2+}/MV^{2+}/[(L_5)Fe^{II}]^{2+}$ under an inert atmosphere shows the rapid formation of a reduced $MV^{\bullet+}$ radical (390 and 605 nm) together with photo-oxidized $[Ru^{III}(bpy)_3]^{3+}$ (bleaching at 450 nm) (Fig. 1A). The classic recombination pathway was validated by the synchronous resetting of these two species to their resting state (Fig. 1B, solid red and blue traces).

We can thus conclude that neither oxidation of the $[(L_5)Fe^{II}]^{2+}$ catalyst by the photo-produced $[Ru^{III}(bpy)_3]^{3+}$ nor its reduction by $MV^{\bullet+}$ occurs in a degassed solution (Fig. 1A). The first process is related to the oxidation of the $[(L_5)Fe^{II}]^{2+}$ catalyst by the photo-produced $[Ru^{III}(bpy)_3]^{3+}$. Although thermodynamically feasible, it was not detected probably because this reaction is slower than back electron transfer from the $MV^{\bullet+}$ radical. A possible reason why the oxidation of $[(L_5)Fe^{II}]^{2+}$ is slow could be due to its oxidation being controlled by deprotonation, which is not favorable at pH 4. The absence of the second process, *i.e.*, the reduction of the $[(L_5)Fe^{II}]^{2+}$catalyst by $MV^{\bullet+}$, is easily explained by the fact that no reduction wave is accessible for the Fe^{II} complex in cyclic voltammetry (Fig. S6†) when scanning down to −1.0 V *vs.* SCE. As such, the reactions occurring under these conditions are identical to those in the absence of the $[(L_5)Fe^{II}]^{2+}$ catalyst (see (i)).

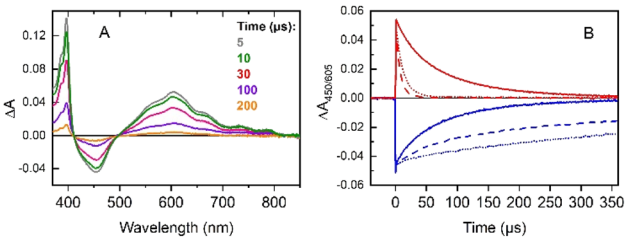

Fig. 1 (A) Transient absorption spectra from an Ar-saturated Britton and Robinson (B&R) pH 4 buffer solution of $[Ru^{II}(bpy)_3]^{2+}$ (30 μM), MV^{2+} (20 mM), and $[(L_5)Fe^{II}]^{2+}$ (100 μM) at the indicated delay times after excitation. (B) Time-resolved absorption changes at 605 nm (red) and 450 nm (blue) in argon-saturated pH 4 buffer (solid), under aerobic conditions (dash), and after renewed excitation under anaerobic conditions of the previous solution (dot).

(v) Under aerobic conditions, we observed the fast disappearance of $MV^{\bullet+}$ (absorption at 605 nm), confirming a rapid electron transfer from the $MV^{\bullet+}$ radical to O_2 to form the superoxide $O_2^{\bullet-}$ anion in aqueous solution (eqn (3), Fig. 1B, dashed red trace).[62,63] In addition, the recovery of the $[Ru^{II}(bpy)_3]^{2+}$ absorption band at 450 nm from the $[Ru^{III}(bpy)_3]^{3+}$ formed is significantly slowed down (Fig. S5†), indicating that back electron transfer from $MV^{\bullet+}$ or $O_2^{\bullet-}$ no longer occurs. This observation can be explained by fast oxidation of $MV^{\bullet+}$ by O_2 as observed (eqn (3)), followed by a preferential reaction of $O_2^{\bullet-}$ with the $[(L_5)Fe^{II}]^{2+}$catalyst (eqn (6)), the concentration of which is much higher than the concentration of $[Ru^{III}(bpy)_3]^{3+}$.

$$[(L_5)Fe^{II}]^{2+} + O_2^{\bullet-} + H^+ \rightarrow [(L_5)Fe^{III}\text{–}OOH]^{2+} \quad (6)$$

Interestingly, in a sequential experiment on a sample first excited in the presence of O_2 and then degassed with argon, the original kinetics observed under anaerobic conditions were not recovered (Fig. 1B, dotted traces). As we can notice, the decay of the $MV^{\bullet+}$ radical was nearly as fast as in the presence of O_2 and the recovery of $[Ru^{II}(bpy)_3]^{2+}$ was very slow. This finding may be attributed to a modification of the $[(L_5)Fe^{III}\text{–}OOH]^{2+}$ complex possibly relaxing to an $[(L_5)Fe^{III}]^{3+}$ species that reacts with the $MV^{\bullet+}$ radical (eqn (7)) under these new anaerobic conditions.

$$MV^{\bullet+} + [(L_5)Fe^{III}]^{3+} \rightarrow MV^{2+} + [(L_5)Fe^{II}]^{2+} \quad (7)$$

The rate constants determined for the different bimolecular interactions are summarized in Table 1. As discussed later, other reactions can also be undergoing to slow down the back electron transfer.

Upon irradiating the triptych mixture of $[Ru^{II}(bpy)_3]^{2+}/MV^{2+}/[(L_5)Fe^{II}]^{2+}$ in the presence of styrene sulfonate in an oxygenated aqueous Britton and Robinson (B&R) pH 4 buffer, two oxygenated products namely diol and benzaldehyde derivatives were detected with an overall TON of *ca.* 70 (Table S1 and Fig. S8†). When the pH of the buffer was fixed at 6, the corresponding epoxide was detected instead of the diol indicating that the ring opening under low pH conditions occurs. The efficiency of the

Table 1 Summary of bimolecular rate constants deduced from laser flash photolysis[a]

Eqn	Reaction	Rate constant (M^{-1} s^{-1})
2	$[Ru^{II}(bpy)_3]^{2+}* + MV^{2+} \rightarrow [Ru^{III}(bpy)_3]^{3+} + MV^{\bullet+}$	0.45×10^9
2′	$[Ru^{III}(bpy)_3]^{3+} + MV^{\bullet+} \rightarrow [Ru^{II}(bpy)_3]^{2+} + MV^{2+}$	3.1×10^9
3	$MV^{\bullet+} + O_2 \rightarrow MV^{2+} + O_2^{\bullet-}$	0.6×10^9
4	$[Ru^{III}(bpy)_3]^{3+} + O_2^{\bullet-} \rightarrow [Ru^{II}(bpy)_3]^{2+} + O_2$	3×10^9
5	$[Ru^{III}(bpy)_3]^{3+} + S \rightarrow [Ru^{II}(bpy)_3]^{2+} + S^{\bullet+}$	8×10^4
7	$MV^{\bullet+} + [(L_5)Fe^{III}]^{3+} \rightarrow MV^{2+} + [(L_5)Fe^{II}]^{2+}$	0.9×10^9

[a] The rate of quenching of the $[Ru^{II}(bpy)_3]^{2+}*$ excited state by MV^{2+} is an apparent rate including the effect of escape yield of about 20%. The bimolecular rate constant for reaction (6) is difficult to estimate given the weak signal of $[(L_5)Fe^{III}–OOH]^{2+}$ under the LFP conditions.

observed photocatalytic reactivity for OAT is comparable with values reported for molecular iron complexes with H_2O_2 as the oxidant.[64] An important control before pursuing further investigation was an $^{18}O_2$ isotopic labelling experiment. The presence of an ^{18}O atom in the high resolution mass spectrometry (HRMS) detected products confirms O_2 as the origin of the oxygen atom under our photocatalytic reaction conditions (Fig. S9 and S10†). Control experiments with only the photosensitizer and the substrate under aerobic conditions did not give any oxidized substrate under irradiation, henceforth, excluding the intervention of singlet O_2 in the observed photocatalytic activity. This experiment also excludes the formation of any decomposed fragments of the photosensitizer that could be responsible for the observed reactivity. The absence of MV^{2+} in the photocatalytic run resulted in no oxygenation reaction, providing solid evidence that the reversible electron carrier is a pre-requisite to carry out the OAT reaction. Photocatalysis in the absence of the iron catalyst or in the presence of $FeCl_3$ instead of the molecular complex led to the formation of traces of the aldehyde supporting the fact that the molecular complex is a necessity for the activation of O_2 and that no prominent radical chemistry is underway (Table S1 and Fig. S8†).

The difficulty in providing insights into a photocatalytic cycle is to capture and characterize any reactive intermediate under light irradiation. This is presumably due to the many events taking place concomitantly under the photocatalytic conditions. One way of solving this issue is to probe the electronic features of the chemically produced active species. According to previous studies,[59,65] the $[(L_5)Fe^{III}–OOH]^{2+}$ species can be followed by a band at 537 nm (in methanol) when chemically generated with an excess of H_2O_2, which is a precursor to active iron-oxo species. With the target to capture the signature of the light-driven formation of the $[(L_5)Fe^{III}–OOH]^{2+}$ species, we followed the changes in the absorption spectrum of the catalyst during the illumination of a mixture of $[Ru^{II}(bpy)_3]^{2+}/MV^{2+}/[(L_5)Fe^{II}]^{2+}$ under aerobic conditions (Fig. 2).

Initially, we opted to use ethylenediaminetetraacetic acid (EDTA) as an electron source. At pH 4 and in the presence of EDTA (Fig. 2a), the loss of the absorption band at 390 nm, characteristic of $[(L_5)Fe^{II}]^{2+}$ (Fig. S11†), is observed together with the appearance of an absorption band around 500 nm, typical of the $[(L_5)Fe^{III}–OOH]^{2+}$ intermediate.[58] The difference spectrum during irradiation therefore represents all features of a light-induced conversion of $[(L_5)Fe^{II}]^{2+}$ to $[(L_5)Fe^{III}–OOH]^{2+}$ (eqn (6)).

The quick decay of the 500 nm band indicates that such a species is very unstable (<1 min) under our experimental conditions. When the same experiment was performed at pH 6, the bleaching of $[(L_5)Fe^{II}]^{2+}$ is correlated with the appearance of a clear signature of the deprotonated peroxo form $[(L_5)Fe^{III}–\eta^2O_2]^+$ with a broad absorption band at around 650 nm (Fig. 2b). EPR spectroscopy was used to further characterize the photogenerated $Fe^{III}–O_2$ species.

Prior to irradiation, the EPR spectrum of the $[Ru^{II}(bpy)_3]^{2+}/MV^{2+}/[(L_5)Fe^{II}]^{2+}$ mixture (Fig. S15,† black trace) shows signals with g values at 4.41 and 4.04 that are assigned to a high spin (HS) $[(L_5)Fe^{III}–X]^{2+}$ species (X being an exogenous ligand such as OH^- based on the electrochemical studies in Fig. S6† or an anion from the buffer) and a signal at 4.27 likely due to a trace of Fe^{3+} impurities.

Upon irradiation of the above mixture in the presence of EDTA as an electron donor and under anaerobic conditions, the signals at 4.41 and 4.04 faded out with the appearance of a signal at $g = 2.00$ very likely originating from the $MV^{\bullet+}$ organic radical

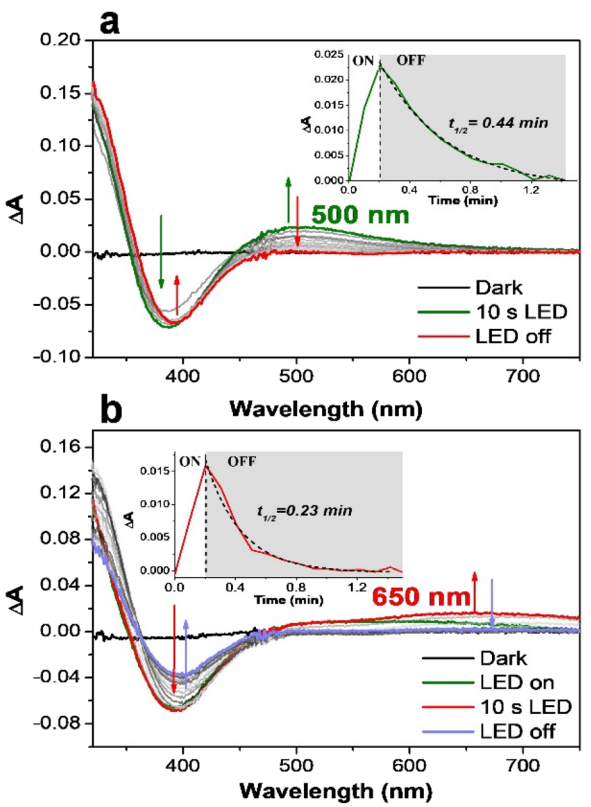

Fig. 2 (a) Spectral evolution of the absorption of a B&R pH 4 buffer solution containing $[Ru^{II}(bpy)_3]^{2+}$ (30 μM), MV^{2+} (10 mM), EDTA (20 mM), and $[(L_5)Fe^{II}]^{2+}$ (100 μM) upon irradiation (100 W m^{-2} for 10 s) under aerobic conditions and no stirring. The difference of absorbance from the solution in the dark and during irradiation. Inset: kinetic profile of the 500 nm band. (b) The same experiment at pH 7.6. Inset: kinetic profile of the 650 nm band.

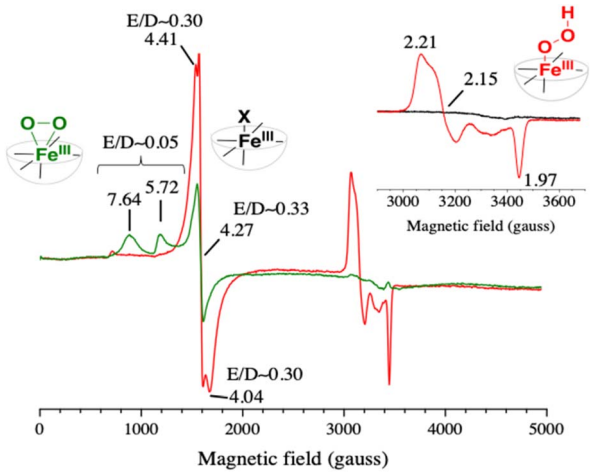

Fig. 3 EPR spectra of a B&R pH 4 buffer solution containing $[Ru^{II}(bpy)_3]^{2+}$ (30 μM), MV^{2+} (20 mM), $[(L_5)Fe^{II}]^{2+}$ (100 μM) and 20 mM EDTA (red) or 200 mM TEOA (green) irradiated for 1 s with a 100 W m^{-2} blue LED. The spectra were recorded at 15 K with a modulation amplitude of 25 gauss and a microwave power of 20 mW (5 mW for the inset). The microwave frequency was ~9.49 GHz. In red, the EPR spectrum of the photo-generated low spin $[(L_5)Fe^{III}–OOH]^{2+}$ species, and in green the EPR spectrum of the photo-generated high spin $[(L_5)Fe^{III}–\eta^2O_2]^+$ species; expanded view shown in Fig. S17.† In the inset, the black spectrum was recorded before the illumination.

(Fig. S15†). This result clearly shows that the HS Fe(III) species can be reduced by $MV^{\bullet+}$. The EPR spectrum after light irradiation for 1 s under an aerobic atmosphere of an aqueous solution containing the triptych mixture buffered at pH 4 and an electron donor (EDTA) showed signals with g values of around 2.21, 2.15 and 1.97, a set of values corresponding to a typical low spin iron(III)-hydroperoxo species (red spectrum in Fig. 3) as described previously.[58] The morphology of this set of signals supports the presence of different rotational isomers of the Fe^{III}–OOH species. We may also note that concomitantly the signals at 4.41 and 4.04 also gain in intensity upon irradiation (Fig. S16†). This can be reasonably attributed to the formation of the same high-spin Fe^{III}–X species present in the initial iron(II) complex that may result from the degradation of the Fe^{III}–OOH intermediate. Furthermore, we found that upon prolonged irradiation time (20 s) both the signals for the Fe^{III}–OOH intermediate and the HS Fe^{III}–X species disappear indicating that $MV^{\bullet+}$ can further reduce the Fe^{III}–OOH catalytic precursor and the HS Fe^{III}–X species to an EPR silent Fe(II) form (Fig. S16†). Such photo-events may also occur to explain the slow recovery of $[Ru^{II}(bpy)_3]^{2+}$ we discussed above.

When the photogeneration was performed in the presence of an excess of triethanolamine (TEOA) (buffer at pH 4 and 200 mM TEOA, resulting in a pH value of 7.26), the EPR spectrum exhibits this time a high spin species with resonances at g = 7.64 and 5.72 (green spectrum in Fig. 3), which indicates the formation of an iron(III)-peroxo $[(L_5)Fe^{III}–\eta^2O_2]^+$ intermediate with S = 5/2 (eqn (6′), see Scheme 2),[58] while the signal at 4.27 for the Fe^{3+} impurity still persists (Fig. S15†).

The same experiment with TEOA as the donor was also performed in the visible absorption and it confirmed both the formation of the characteristic band of the iron(III)-peroxo species at 650 nm and the accumulation of $MV^{\bullet+}$ once the O_2 was locally consumed (Fig. S13†). Based on these results, we can conclusively support that the photochemically produced $[(L_5)Fe^{III}–OOH]^{2+}$ and $[L_5Fe^{III}–\eta^2O_2]^+$ species match the electronic signatures of the chemically generated ones. When conducted with 4-styrene sulfonate as the electron donor to $[Ru^{III}(bpy)_3]^{3+}$, the observed spectral changes were not as notable as with EDTA, which is a better electron donor. However, the same trend of spectral modifications in the absorption spectra was observed (Fig. S12†). The low spin Fe^{III}–OOH species was also evidenced albeit with lower intensities.

At this point, gathering all the photophysical events we can reasonably propose a photocatalytic cycle to explain the OAT reaction, as summarized in Scheme 2. It is noteworthy that in the photocatalytic runs no sacrificial electron donor was needed to perform the OAT reaction as described below. The first photophysical event concerns the generation of the charge separated state described by $MV^{\bullet+}$–$[Ru^{III}(bpy)_3]^{3+}$ (eqn (2)). From here, $MV^{\bullet+}$ reacts with O_2 to form $O_2^{\bullet-}$ (eqn (3)), leaving behind an oxidizing equivalent of $[Ru^{III}(bpy)_3]^{3+}$. The $O_2^{\bullet-}$ can react with the starting Fe(II) complex to form after protonation $[(L_5)Fe^{III}–OOH]^{2+}$ (eqn (6)) in the catalytic cycle, while $[Ru^{III}(bpy)_3]^{3+}$ can oxidize the alkene substrate to form an alkenyl radical species (eqn (5)). According to in-depth mechanistic studies albeit in organic solvents, $[(L_5)Fe^{III}–OOH]^{2+}$ can evolve to an iron-oxo species that enables the oxygen atom transfer reaction to the alkene to form an epoxide or a diol derivative as reported.[8,66,67] Isotopic labelling experiments carried out in the presence of $^{18}O_2$ produced the corresponding labeled and unlabeled epoxide at pH 6, suggesting the involvement of a high-valent iron-oxo species prone to O-atom exchange with the water solvent molecules. At pH 4, the diol derivative is detected with a double ^{18}O, a mixed ^{18}O and ^{16}O and a double ^{16}O content (Fig. S9 and Scheme S1†). Such an observation can be explained by the *cis*-hydroxylation of the alkene substrate by an iron-oxo-hydroxo intermediate or the formation of the epoxide, followed by a ring opening process with unlabeled water molecules (eqn (8), see Scheme 2).

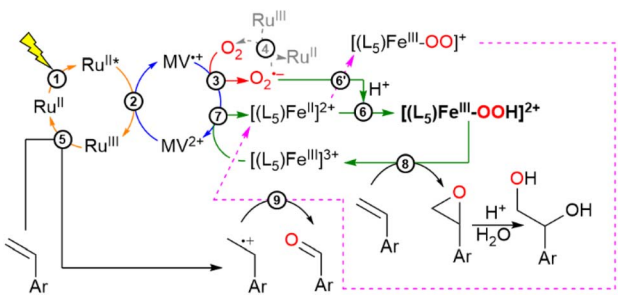

Scheme 2 Photocatalytic OAT to an alkene substrate in the absence of a sacrificial electron donor using light, O_2 as the oxygen source, $[(L_5)Fe^{II}]^{2+}$ as the catalyst, $[Ru^{II}(bpy)_3]^{2+}$ as the photosensitizer (written as Ru^{II} for simplification) and MV^{2+} as the electron relay. Reaction numbers refer to equation numbers in the discussion.

The detected aldehyde may derive from the reaction of the alkenyl radical with the reactive $[L_5Fe^{III}–\eta^2O_2]^+$ to form an unstable dioxetane ring that after cleavage leads to the corresponding aldehyde (eqn (9), see Scheme 2; further details in Scheme S1†).[8] An important mechanistic aspect concerns the evolution of $[(L_5)Fe^{III}–OOH]^{2+}$ leading to either Fe(v)O or Fe(iv)O following a heterolytic or homolytic cleavage scheme of the O–O bond of the catalytic precursor in an aqueous medium.[20] These proposed mechanisms are based on the abundant work in this field and are recalled in the ESI (Scheme S1).† Accordingly, under these scenarios, either Fe(iii) or Fe(ii) would result after the OAT reaction to be refurnished in the catalytic cycle. Studies from Que and colleagues have shown that the presence of water would enhance the heterolytic bond cleavage in a molecular Fe^{III}–OOH intermediate.[20] In this present study, we can only speculate on such an issue as none of these high-valent iron oxo species have been characterized under our experimental conditions. Interestingly, from the EPR spectrum of the photogenerated low spin $[(L_5)Fe^{III}–OOH]^{2+}$, we also observed a gain in the intensity of the signals of the high spin Fe(iii) species that we argued to stem from the degradation of the $[(L_5)Fe^{III}–OOH]^{2+}$ intermediate (Fig. S16†). Henceforth, it is more likely that the active species is actually Fe(v)O that would yield an Fe(iii) species after the OAT reaction to re-enter the catalytic loop to be reduced by $MV^{\bullet+}$ (eqn (7)). This electron transfer process is thermodynamically feasible as confirmed by the redox properties of the iron complex in an aqueous medium, where two observed cathodic peaks are assigned tentatively to the couples $([(L_5)Fe^{III}–OH_2]^{3+}/[(L_5)Fe^{II}–OH_2]^{2+}) = 0.13$ V *vs.* SCE and $([(L_5)Fe^{III}–OH]^{2+}/[(L_5)Fe^{II}–OH]^{+}) = -0.17$ V *vs.* SCE (Fig. S6†) compared to $E^0(MV^{2+}/MV^{\bullet+}) = -0.69$ V *vs.* SCE. Further investigation on this segment of the catalytic cycle will be needed to clarify the actual nature of the catalytically active iron-oxo species in an aqueous medium.

Conclusions

In this study, we have shown a scenario where sharing the two-electron activation of O_2 on both O_2 and a non-heme Fe(iii) catalyst allows us to avoid the charge accumulation process. EPR spectroscopy and LFP data backed the metal centered activity with the unprecedented interception of a light-driven formation of an Fe^{III}–OOH species in the OAT reaction that rules out an auto-oxidation pathway. Another attractive feature of this study concerns the elimination of sacrificial electron donors that still prohibit any value-added synthetic procedure.[68,69] For the overall efficiency of the photocatalytic system, it is important that productive reaction steps are competitive with respect to alternative short-circuit reactions. Two such "crossroads" can be easily identified as the preferential reduction of the resulting $[(L_5)Fe^{III}–OH]^{2+}$ state *vs.* reduction of the catalytically active $[(L_5)Fe^{III}–OOH]^{2+}$ state and the preferential oxidation by Ru(iii) of the substrate *vs.* oxidation of the $[(L_5)Fe^{II}]^{2+}$ state. Another point that needs to be further investigated concerns the reactivity of the generated alkenyl radical.[70–73] An alternative route to preclude such a pathway may reside in tandem oxidation reactions with different organic substrates. These challenges are currently being addressed.

Data availability

The datasets supporting this article have been uploaded as part of the ESI.†

Author contributions

Eva Pugliese: formal analysis and investigation. Nhat Tam Vo: formal analysis and investigation. Alain Boussac: formal analysis and investigation. Fréderic Banse: formal analysis. Yasmina Mekmouche: investigation. Jalila Simaan: investigation. Thierry Tron: investigation and funding acquisition. Philipp Gotico: formal analysis and investigation. Marie Sircoglou: formal analysis. Zakaria Halime: formal analysis, investigation, and data curation. Winfried Leibl: formal analysis, investigation, funding acquisition, data curation, and writing of the original draft. Ally Aukauloo: lead formal analysis, funding acquisition, writing of the original draft, and project administration.

Conflicts of interest

There are no conflicts to declare.

Acknowledgements

French National Research Agency ANR Multiplet (ANR-15-CE07-0021-01), E.P. thanks ANR LOCO, grant No: ANR-19-CE05-0020-02. We thank LABEX CHARMMMAT, grant No: ANR-11-LABX-0039).

Notes and references

1 P. R. Ortiz de Montellano, *Chem. Rev.*, 2010, **110**, 932–948.
2 T. L. Poulos, *Chem. Rev.*, 2014, **114**, 3919–3962.
3 X. Huang and J. T. Groves, *Chem. Rev.*, 2018, **118**, 2491–2553.
4 C. Krebs, D. Galonić Fujimori, C. T. Walsh and J. M. Bollinger, *Acc. Chem. Res.*, 2007, **40**, 484–492.
5 J. P. T. Zaragoza and D. P. Goldberg, *Dioxygen-dependent Heme Enzymes*, The Royal Society of Chemistry, 2019, 1–36.
6 M. Costas, M. P. Mehn, M. P. Jensen and L. Que, *Chem. Rev.*, 2004, **104**, 939–986.
7 S. Fukuzumi, K.-B. Cho, Y.-M. Lee, S. Hong and W. Nam, *Chem. Soc. Rev.*, 2020, **49**, 8988–9027.
8 W. N. Oloo and L. Que, *Acc. Chem. Res.*, 2015, **48**, 2612–2621.
9 S. Dey, B. Mondal, S. Chatterjee, A. Rana, S. Amanullah and A. Dey, *Nat. Rev. Chem.*, 2017, **1**, 1–20.
10 W. Nam, *Acc. Chem. Res.*, 2007, **40**, 465.
11 S. Friedle, E. Reisner and S. J. Lippard, *Chem. Soc. Rev.*, 2010, **39**, 2768–2779.
12 J. T. Groves, *J. Inorg. Biochem.*, 2006, **100**, 434–447.
13 C. E. Tinberg and S. J. Lippard, *Acc. Chem. Res.*, 2011, **44**, 280–288.
14 F. Li, J. England and L. Que, *J. Am. Chem. Soc.*, 2010, **132**, 2134–2135.
15 Y.-M. Lee, S. Hong, Y. Morimoto, W. Shin, S. Fukuzumi and W. Nam, *J. Am. Chem. Soc.*, 2010, **132**, 10668–10670.

16 J. Yoon, S. A. Wilson, Y. K. Jang, M. S. Seo, K. Nehru, B. Hedman, K. O. Hodgson, E. Bill, E. I. Solomon and W. Nam, *Angew. Chem., Int. Ed.*, 2009, **48**, 1257–1260.
17 L. Que, *Acc. Chem. Res.*, 2007, **40**, 493–500.
18 A. Thibon, J. England, M. Martinho, V. G. Young Jr, J. R. Frisch, R. Guillot, J.-J. Girerd, E. Münck, L. Que Jr and F. Banse, *Angew. Chem., Int. Ed.*, 2008, **47**, 7064–7067.
19 J. Cho, S. Jeon, S. A. Wilson, L. V. Liu, E. A. Kang, J. J. Braymer, M. H. Lim, B. Hedman, K. O. Hodgson, J. S. Valentine, E. I. Solomon and W. Nam, *Nature*, 2011, **478**, 502–505.
20 W. N. Oloo, A. J. Fielding and L. Que, *J. Am. Chem. Soc.*, 2013, **135**, 6438–6441.
21 J.-J. Girerd, F. Banse and A. J. Simaan, in *Metal-Oxo and Metal-Peroxo Species in Catalytic Oxidations*, ed. B. Meunier, Springer, Berlin, Heidelberg, 2000, 145–177.
22 M. Martinho, P. Dorlet, E. Rivière, A. Thibon, C. Ribal, F. Banse and J.-J. Girerd, *Chem.–Eur. J.*, 2008, **14**, 3182–3188.
23 S. E. Creager, S. A. Raybuck and R. W. Murray, *J. Am. Chem. Soc.*, 1986, **108**, 4225–4227.
24 M. Mukherjee and A. Dey, *ACS Cent. Sci.*, 2019, **5**, 671–682.
25 N. Kostopoulos, C. Achaibou, J.-M. Noël, F. Kanoufi, M. Robert, C. Fave and E. Anxolabéhère-Mallart, *Inorg. Chem.*, 2020, **59**, 11577–11583.
26 J.-M. Noel, N. Kostopoulos, C. Achaibou, C. Fave, E. Anxolabéhère-Mallart and F. Kanoufi, *Angew. Chem., Int. Ed.*, 2020, **59**, 16376–16380.
27 N. Ségaud, E. Anxolabéhère-Mallart, K. Sénéchal-David, L. Acosta-Rueda, M. Robert and F. Banse, *Chem. Sci.*, 2014, **6**, 639–647.
28 R. Oliveira, W. Zouari, C. Herrero, F. Banse, B. Schöllhorn, C. Fave and E. Anxolabéhère-Mallart, *Inorg. Chem.*, 2016, **55**, 12204–12210.
29 E. Anxolabéhère-Mallart and F. Banse, *Curr. Opin. Electrochem.*, 2019, **15**, 118–124.
30 A. L. Robinson, J.-N. Rebilly, R. Guillot, C. Herrero, H. Maisonneuve and F. Banse, *Chem.–Eur. J.*, 2022, **28**, e202200217.
31 M. E. Ener, Y.-T. Lee, J. R. Winkler, H. B. Gray and L. Cheruzel, *Proc. Natl. Acad. Sci. U. S. A.*, 2010, **107**, 18783–18786.
32 L. Marzo, S. K. Pagire, O. Reiser and B. König, *Angew. Chem., Int. Ed.*, 2018, **57**, 10034–10072.
33 C. K. Prier, D. A. Rankic and D. W. C. MacMillan, *Chem. Rev.*, 2013, **113**, 5322–5363.
34 S. Fukuzumi, T. Kishi, H. Kotani, Y.-M. Lee and W. Nam, *Nat. Chem.*, 2011, **3**, 38–41.
35 X. Wu, X. Yang, Y.-M. Lee, W. Nam and L. Sun, *Chem. Commun.*, 2015, **51**, 4013–4016.
36 H. Kotani, T. Suenobu, Y.-M. Lee, W. Nam and S. Fukuzumi, *J. Am. Chem. Soc.*, 2011, **133**, 3249–3251.
37 S. Fukuzumi, S. Kuroda and T. Tanaka, *J. Am. Chem. Soc.*, 1985, **107**, 3020–3027.
38 J. Berglund, T. Pascher, J. R. Winkler and H. B. Gray, *J. Am. Chem. Soc.*, 1997, **119**, 2464–2469.
39 W. Zhang, E. Fernández-Fueyo, Y. Ni, M. van Schie, J. Gacs, R. Renirie, R. Wever, F. G. Mutti, D. Rother, M. Alcalde and F. Hollmann, *Nat. Catal.*, 2018, **1**, 55–62.
40 C. Herrero, A. Quaranta, M. Sircoglou, K. Sénéchal-David, A. Baron, I. M. Marín, C. Buron, J.-P. Baltaze, W. Leibl, A. Aukauloo and F. Banse, *Chem. Sci.*, 2015, **6**, 2323–2327.
41 C. Panda, J. Debgupta, D. Díaz Díaz, K. K. Singh, S. Sen Gupta and B. B. Dhar, *J. Am. Chem. Soc.*, 2014, **136**, 12273–12282.
42 B. Chandra, K. K. Singh and S. S. Gupta, *Chem. Sci.*, 2017, **8**, 7545–7551.
43 C. Herrero, A. Quaranta, R. Ricoux, A. Trehoux, A. Mahammed, Z. Gross, F. Banse and J.-P. Mahy, *Dalton Trans.*, 2015, **45**, 706–710.
44 B. Mühldorf, U. Lennert and R. Wolf, *Phys. Sci. Rev.*, 2019, **4**, 20180030.
45 F. Avenier, C. Herrero, W. Leibl, A. Desbois, R. Guillot, J.-P. Mahy and A. Aukauloo, *Angew. Chem., Int. Ed.*, 2013, **52**, 3634–3637.
46 J. Chen and W. R. Browne, *Coord. Chem. Rev.*, 2018, **374**, 15–35.
47 J. Rosenthal, T. D. Luckett, J. M. Hodgkiss and D. G. Nocera, *J. Am. Chem. Soc.*, 2006, **128**, 6546–6547.
48 S. Bang, Y.-M. Lee, S. Hong, K.-B. Cho, Y. Nishida, M. S. Seo, R. Sarangi, S. Fukuzumi and W. Nam, *Nat. Chem.*, 2014, **6**, 934–940.
49 J. Jung, K. Ohkubo, D. P. Goldberg and S. Fukuzumi, *J. Phys. Chem. A*, 2014, **118**, 6223–6229.
50 R. Cibulka, R. Vasold and B. König, *Chem.–Eur. J.*, 2004, **10**, 6223–6231.
51 B. Mühldorf and R. Wolf, *Angew. Chem., Int. Ed.*, 2016, **55**, 427–430.
52 H. D. Gafney and A. W. Adamson, *J. Am. Chem. Soc.*, 1972, **94**, 8238–8239.
53 K. Kalyanasundaram, *Coord. Chem. Rev.*, 1982, **46**, 159–244.
54 H. Sun, A. Yoshimura and M. Z. Hoffman, *J. Phys. Chem.*, 1994, **98**, 5058–5064.
55 M. Z. Hoffman, D. R. Prasad, G. Jones and V. Malba, *J. Am. Chem. Soc.*, 1983, **105**, 6360–6362.
56 K. Z. Ismail and S. G. Weber, *Biosens. Bioelectron.*, 1991, **6**, 699–705.
57 J. J. Orgill, C. Chen, C. R. Schirmer, J. L. Anderson and R. S. Lewis, *Biochem. Eng. J.*, 2015, **94**, 15–21.
58 A. J. Simaan, S. Döpner, F. Banse, S. Bourcier, G. Bouchoux, A. Boussac, P. Hildebrandt and J.-J. Girerd, *Eur. J. Inorg. Chem.*, 2000, **2000**, 1627–1633.
59 A. Bohn, C. Chinaux-Chaix, K. Cheaib, R. Guillot, C. Herrero, K. Sénéchal-David, J.-N. Rebilly and F. Banse, *Dalton Trans.*, 2019, **48**, 17045–17051.
60 A. Bohn, PhD thesis, Université Paris Saclay (COmUE), 2018, accessible at **https://tel.archives-ouvertes.fr/tel-02018125**.
61 R. Farran, Y. Mekmouche, N. T. Vo, C. Herrero, A. Quaranta, M. Sircoglou, F. Banse, P. Rousselot-Pailley, A. J. Simaan, A. Aukauloo, T. Tron and W. Leibl, *iScience*, 2021, **24**(4), 102378.
62 D. T. Sawyer and J. S. Valentine, *Acc. Chem. Res.*, 1981, **14**, 393–400.

63 Y. Nosaka and A. Y. Nosaka, *Chem. Rev.*, 2017, **117**, 11302–11336.
64 G. Olivo, O. Cussó, M. Borrell and M. Costas, *J. Biol. Inorg Chem.*, 2017, **22**, 425–452.
65 I. Bernal, I. M. Jensen, K. B. Jensen, C. J. McKenzie, H. Toftlund and J.-P. Tuchagues, *J. Chem. Soc., Dalton Trans.*, 1995, 3667–3675.
66 I. Gamba, Z. Codolà, J. Lloret-Fillol and M. Costas, *Coord. Chem. Rev.*, 2017, **334**, 2–24.
67 Y. Feng, J. England and L. Que, *ACS Catal.*, 2011, **1**, 1035–1042.
68 N. T. Vo, Y. Mekmouche, T. Tron, R. Guillot, F. Banse, Z. Halime, M. Sircoglou, W. Leibl and A. Aukauloo, *Angew. Chem., Int. Ed.*, 2019, **58**, 16023–16027.
69 Y. Pellegrin and F. Odobel, *C. R. Chim.*, 2017, **20**, 283–295.
70 L. M. Smith, H. M. Aitken and M. L. Coote, *Acc. Chem. Res.*, 2018, **51**, 2006–2013.
71 Y.-F. Liang and N. Jiao, *Acc. Chem. Res.*, 2017, **50**, 1640–1653.
72 L. J. Johnston and N. P. Schepp, *J. Am. Chem. Soc.*, 1993, **115**, 6564–6571.
73 L. J. Johnston and N. P. Schepp, *Pure Appl. Chem.*, 1995, **67**, 71–78.